Laser and Particle Beams (2002), *20*, 269–275. Printed in the USA.

DOI: 10.1017/S0263034602202177

Laser-produced protons and their application as a particle probe

M. BORGHESI,[1] D. H. CAMPBELL,[2] A. SCHIAVI,[2] O. WILLI,[3] A. J. MACKINNON,[4] D. HICKS,[4] P. PATEL,[4] L. A. GIZZI,[5] M. GALIMBERTI,[5] AND R. J. CLARKE[6]

[1]Department of Pure and Applied Physics, The Queen's University of Belfast, Belfast BT7 1NN, UK
[2]The Blackett Laboratory, Imperial College, London, UK
[3]Institut für Laser- und Plasmaphysik, Heinrich-Heine-Universität, Düsseldorf, Germany
[4]Lawrence Livermore National Laboratory, Livermore, CA, USA
[5]Intense Laser Irradiation Laboratory, IFAM-CNR, Pisa, Italy
[6]Central Laser Facility, Rutherford Appleton Laboratory, Chilton, UK

(RECEIVED 14 November 2001; ACCEPTED 3 December 2001)

Abstract

One of the most exciting results recently obtained in the ultraintense interaction research area is the observation of beams of protons with energies up to several tens of megaelectron volts, generated during the interaction of ultraintense picosecond pulses with solid targets. The particular properties of these beams (high brilliance, small source size, high degree of collimation, short duration) make them of exceptional interest in view of diagnostic applications. In a series of experiments carried out at the Rutherford Appleton Laboratory (RAL) and at the Lawrence Livermore National Laboratory (LLNL), the laser-produced proton beams have been characterized in view of their application as a particle probe for high-density matter, and applied to diagnose ultraintense laser–plasma interactions. In general, the intensity cross section of a proton beam traversing matter will be modified both by collisional stopping/scattering, and deflections caused by electric/magnetic fields. With a suitable choice of irradiation geometry and target parameters, the proton probe can be made mainly sensitive to the electric field distribution in the object probed. Therefore, point projection proton imaging appears as a powerful and unique technique for electric field detection in laser-irradiated targets and plasmas. The first measurements of transient electric fields in high-intensity laser-plasma interactions have been obtained with this technique.

Keywords: e.m. fields diagnosis; Laser–plasma interaction; Particle acceleration

1. INTRODUCTION

One of the most exciting results recently obtained in laser–plasma interaction experiments is the observation of very energetic beams of protons, generated during the interaction of ultraintense short pulses with solid targets. In a number of experiments, performed with different laser systems and in different interaction conditions, protons with energies up to several tens of megaelectron volts have been detected behind thin foils irradiated with high intensity pulses (Clark *et al.*, 2000; Maksimchuk *et al.*, 2000; Snavely *et al.*, 2000). In these experiments, it was seen that the particle beams are directed along the normal to the back surface of the target, and are remarkably collimated at the highest energies. These characteristics distinguish these beams from the less directed, lower energy protons observed in earlier work at lower intensities (Gitomer *et al.*, 1984; Fews *et al.*, 1994). As proton beams are observed even using targets which nominally do not contain hydrogen, protons are thought to originate from hydrocarbon impurities located on the target surfaces (Gitomer *et al.*, 1984) or from bulk contamination of the target. Since the first observations of the proton beams, there have been conflicting interpretations of the available experimental evidence, and different theoretical models of the origin of these protons have emerged. In particular, there is a strong ongoing debate about whether the source of the energetic protons is located at the front or at the back surface of the solid target. Arguments based on the angular distributions of the proton energy across the beam (observation of mono-energetic proton rings) have been used to support the hypothesis of a proton source located at the front surface of the target (Clark *et al.*, 2000). The possible role of accelerating fields inside the target has been recently proposed (Zepf *et al.*, 2001) as a mean of explaining the results of these experiments. A front-surface acceleration mechanism

Address correspondence and reprint requests to: M. Borghesi, Department of Pure and Applied Physics, The Queen's University of Belfast, Belfast BT7 1NN, UK. E-mail: m.borghesi@qub.ac.uk

(Maksimchuk *et al.*, 2000) has been proposed by another group to explain nuclear activation results obtained using targets overcoated with deuterated plastic layers (Nemoto *et al.*, 2001).

Among the arguments supporting the proton acceleration at the back of the target, there is the fact that the proton beam is perpendicular to the target back surface, rather than collinear with the interaction beam (Snavely *et al.*, 2000). Furthermore, one recent experiment (Mackinnon *et al.*, 2001*a*) has shown that the proton beam can be eradicated by introducing a small preformed plasma at the rear of the target, demonstrating that the protons observed in this experiment were accelerated at the back of the target. In this model, the protons are accelerated by the enormous electric field (~MV/micron) set up by the fast electrons trapped in the Debye sheath at the back surface (Hatchett *et al.*, 2000; Pukhov, 2001; Ruhl *et al.*, 2001). Three-dimensional PIC simulations have shown that the highest energy protons are accelerated at the rear surface, and have reproduced the mono-energetic rings purely as an effect of the Debye sheath geometry (Pukhov, 2001).

Overall, the lack of a unified view on the proton generation mechanism may depend on the wide range of target and laser parameters used in the experimental tests which have been performed. It is reasonable that the dominance of a generation mechanism on the other will strongly depend on features such as, for example, target thickness and composition, or the main-to-prepulse contrast ratio of the interaction pulse.

In any case, the proton beams generated via ultraintense interaction in all the experiments mentioned above present some common characteristics (small source size, high degree of collimation, short duration, energy dependence on the target characteristics) that make them unique, and very desirable in view of applications. In particular, we have explored their use as a particle probe in laser plasma experiments. In this paper, we will first review the properties of the proton beams observed in a series of experiments, performed partly using the VULCAN laser facility at the Rutherford Appleton Laboratory, partly using the JanUSP at the Lawrence Livermore National Laboratory. We will then present the diagnostic setup employed to probe laser–plasma interaction experiments, and finally we will briefly discuss some of the first results obtained with this probing setup.

2. PROTON BEAM CHARACTERISTICS

The protons were mainly produced by focusing the ultraintense laser pulses onto Al foils. These targets were chosen for ease of use and fabrication, and also because, in comparison with targets containing hydrogen as a main constituent (e.g., plastic foils), the proton beams produced were more spatially uniform, while covering the same energy range. The parameters of the lasers used for proton production were as follows. The VULCAN laser, operating in the Chirped Pulse Amplification mode (CPA), provides 1.054-μm, 1-ps pulses with energy up to 100 J. When focused on target by an $f/3.5$ off-axis parabola (OAP; usually p-polarised, at a 15° incidence with the target normal), the focal spot varied between 8 and 10 μm in diameter at full width at half maximum (FWHM), containing 30–40% of the energy, and giving intensities up to $5–7 \times 10^{19}$ W/cm^2. The main-to-prepulse contrast ratio of the VULCAN CPA laser is estimated to be around 10^6:1. The CPA JanUSP pulse at LLNL has a wavelength of 0.8 μm and 100 fs duration. It was focused on target by an f/2 OAP, p-polarised, at an angle of incidence of 22°, with a focal spot of 3–5 μm, FWHM. This spot contained 30–40% of the energy, giving a peak intensity in excess of 10^{20} W/cm^2. The laser used an ASE suppression system to attain an intensity contrast ratio of 10^{10}:1.

In experiments at both facilities, the protons were detected using layers of radiochromic film (RCF, a detector of absorbed dose; McLaughlin *et al.*, 1991) and CR39 (a plastic nuclear track detector; Fews and Henshaw, 1982), which were placed in a stack at the back of the target, typically at a distance of about 2 cm. The diagnostic setup is shown in Figure 1, together with the layout of a single RCF layer of the type used in our experiments (Gafchromic MD55D). Figure 1a shows that objects/plasmas could be placed between the source and the detector. In the following, we will explicitly say when this was the case. However, in most of the proton beam characterization studies, the protons were left free to propagate to the detector without obstructions. As shown in Figure 1b, the film consisted of an ~270-μm-thick plastic containing a double layer of organic dye, which reacts to ionizing radiation. The equivalent dose of energetic protons stopped in the film can be measured from the changes in optical density undergone by the film, yielding information on the number and energy of the protons. By stacking them as indicated in Figure 1a, each layer of film acts as a filter for the following layers. Since protons deposit energy mainly in the Bragg peak at the end of their range, each RC film layer spectrally selects a narrow interval of proton energies. There is therefore a correspondence between the position of the layer and the minimum energy of the protons contributing to the signal in the layer. The first RCF layer was shielded with an Al foil (typically 25 μm in thickness), to stop scattered laser light from reaching the detector pack. The Al foil is also sufficient to prevent the slow moving, higher-Z ions from reaching the following RCF layers. In some shots, CR39 layers were inserted in between the RC film layers. CR39 is a polymer particle detector in which energetic ions cause damage as they transit through it. Subsequent etching is then carried out to reveal the ion tracks as etched holes. This was used to confirm that the energy deposited in the preceding RCF layers was due to protons, and not, for example, to electrons or X-rays to which the RCF is also sensitive.

In both experiments, bright proton beams were produced, although the numbers varied significantly in the experiments carried out with the two lasers. On VULCAN, there

https://doi.org/10.1017/S0263034602202177 Published online by Cambridge University Press

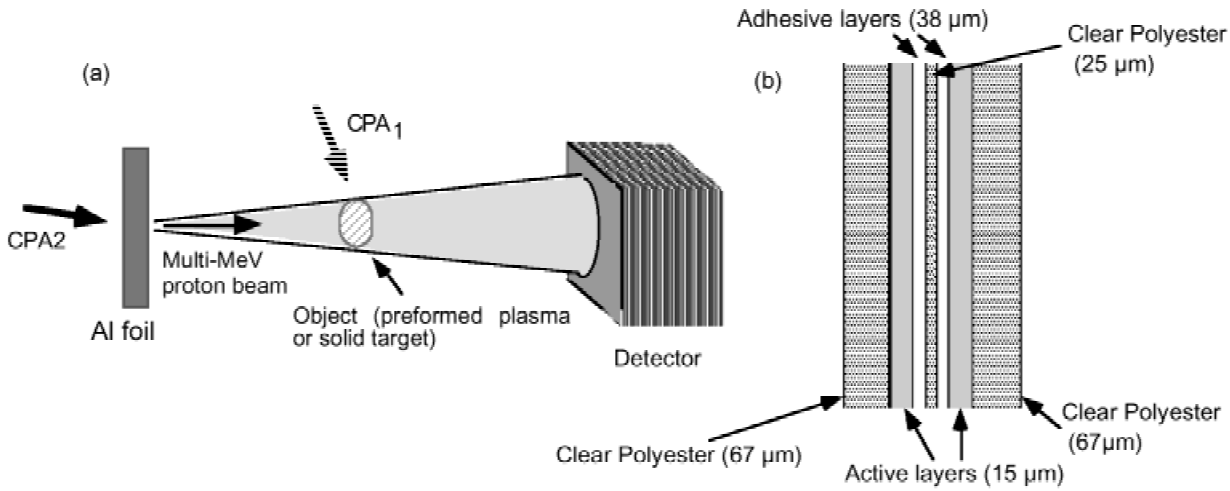

Fig. 1. (a) Experimental setup for proton imaging. The CPA_1 laser pulse was used to produce the proton beam. In part of the campaign, a second CPA pulse (CPA_2) was available and focused on the object target in order to produced highly transient fields. (b) Layout of a layer of Gafchromic MD55 RCF.

were typically more than 10^{12} protons per shot with energy above 3 MeV (for laser irradiances higher than 5×10^{19} W/cm^2). On JanUSP, the number of protons per shot was about an order of magnitude lower.

The spectral content and divergence of the beams obtained on the two systems was comparable, but depended on the thickness of the targets used, with the proton energy generally decreasing as the thickness was increased (Mackinnon *et al.*, 2001*b*).

As an example, when using on VULCAN 25-μm-thick Al foils (a thickness that guaranteed both high energies and spatial uniformity), a proton signal was observed out to the layer corresponding to proton energy above 25 MeV. The energy deposited within each film layer can be extracted from the absolutely calibrated film. This is done for each film layer, giving the energy deposited by the protons stopping in the various layers. By fitting these points with an exponential energy dependence, an estimate of the proton energy spectrum and total energy can be extracted from the film data. On a typical shot, the mean proton energy of the exponential fit was about 3.5 MeV with a total energy of about 2 J in an equivalent Maxwellian. For comparison, shots from 3-μm Al foils at JanUSP gave about the same results (temperature of 3 MeV and maximum energy between 20 and 25 MeV).

The beams are well collimated, as visible in Figure 2, where the half angle of proton emission is plotted versus the proton energy for two Vulcan shots (using 25 μm and 250 μm Al targets). The angular aperture decreases with the proton energy, and generally beams from thicker targets were better collimated. Similar results were obtained on JanUSP (the emission angle from a 3-μm foil varied from about 18° for 8-MeV protons to 7° for 18-MeV protons).

In view of probing application, a most important issue is represented by the size of the proton source, as this will determine the spatial resolution of the probe data. During the experiments, the source size of the proton beam was estimated using various methods, including penumbral edge techniques. These methods imply placing a thick edge (thicker than the stopping distance of the protons) on the way of the beam and infer the source size from the steepness of the penumbral region at the edge of the shadow. However, in our experiments, it was observed that any object placed in the path of the beam charges up positively, likely due to precursor electrons also emitted from the target. In general, this will affect edge measurements and lead to an overestimate of the source size. With this method, we obtained an upper limit of 10 μm for the source of 10-MeV protons (the source size also decreases at increasing energies).

The observed charge-up of objects placed in the beam path led to the possibility of impressing a shadow in the proton beam profile even with objects much thinner than the proton collisional stopping distance. This phenomenon proved to be extremely useful for investigating the properties of the source. Figure 3a shows the shadow impressed by a mesh made of 5 μm Au wires with 20-μm spacing in the profile of the proton beam produced with the JanUSP laser (the layer shown is the third, corresponding to 8-MeV protons). In Figure 3b, the profile of optical density across three periods of the shadow of the mesh is shown. The shadow is seen because the electric field near the surface of the wires deflects the protons away. Therefore a minimum in absorbed dose will be observed in the RCF in correspondence with the position of the wires of the mesh, and by looking at the size of the shadow we can deduce information on the source size. Since the FWHM of the shadow is 8 μm, the blurring caused by the source size cannot be larger than 3 μm, which we can take as an upper limit of the source size for the 8-MeV protons.

https://doi.org/10.1017/S0263034602202177 Published online by Cambridge University Press

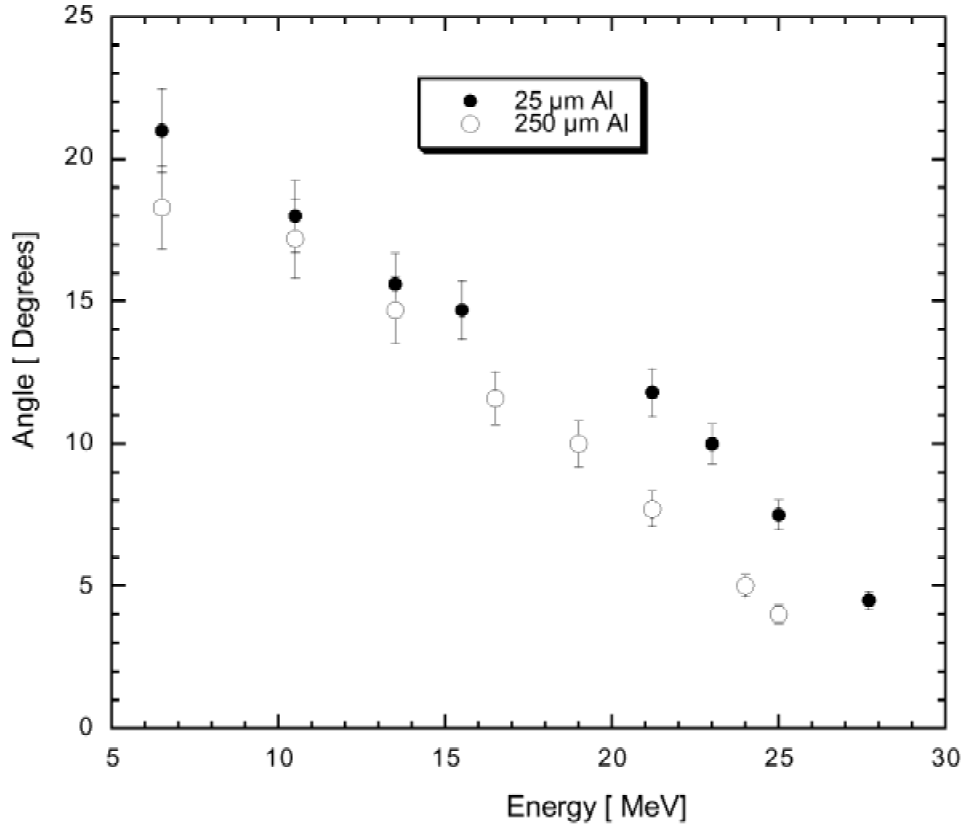

Fig. 2. Angular aperture (half-angle) of the proton components of the beam plotted versus their energy for two different VULCAN shots (respectively, using 25-μm- and 250-μm-thick Al foils as the proton source).

The observation of the mesh magnification on the detector provides important information on the nature of the source. Due to the small source size, the shadow of the mesh can be seen as a point projection image. If the source were located at the plane of the target, the magnification would be given by $M_G = 1 + L/d$, with d and L, respectively, the source-to-object and object-to-detector distances. However, the magnification is consistently lower than this value. We

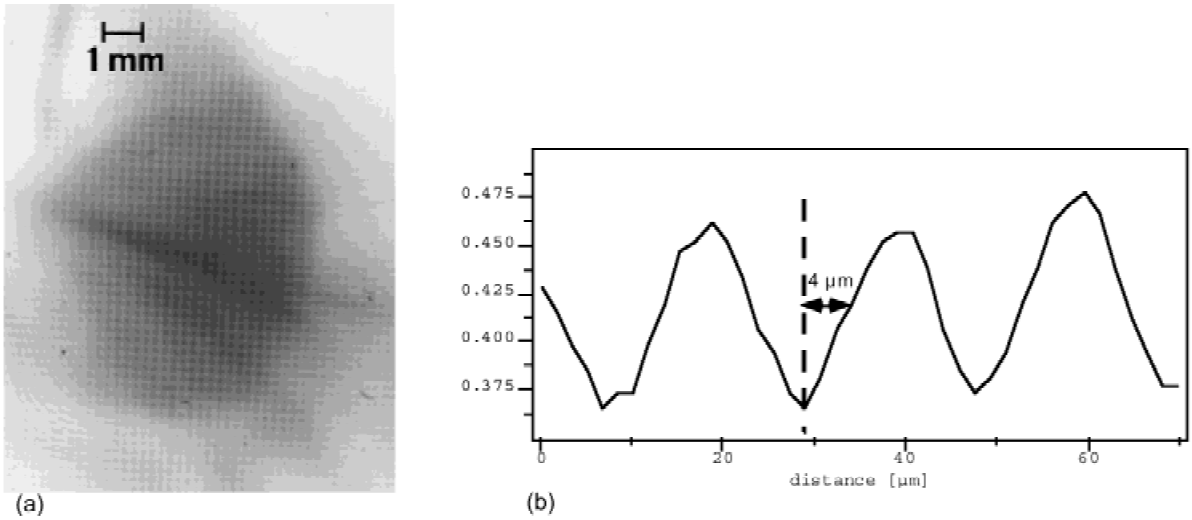

Fig. 3. (a) Shadow of a 5-μm Au wire mesh with 20-μm separation, obtained with 8 MeV protons onto RC film. (b) Lineout of optical density across the mesh shadow.

https://doi.org/10.1017/S0263034602202177 Published online by Cambridge University Press

believe that this is an indication that the source is virtual and placed a distance x before the target. In this case the magnification would be given by $M_{exp} = 1 + L/(d + x) < M_G$. The deviation of the magnification observed experimentally from M_G is consistent with $x \sim 400$ μm. This implies that the protons are emitted from a region of the target much larger than the source size, but with a fixed divergence. For example, taking an emittance half-angle of 15°, the diameter of the region emitting the protons would be around 200 μm. Incidentally, this may help to explain the large number of protons observed even from a metallic target (which would be inconsistent with a micron-sized source).

Another property of fundamental importance for probing application is the short duration of the proton pulse. In the Debye-sheath acceleration model, the pulse duration is determined by the fast electrons' energy depletion time (Hatchett *et al.*, 2000). PIC simulations indicate that this time is of the order of the laser pulse duration. In our experiment, the pulse duration was observed to be less than 5 ps (Borghesi *et al.*, 2001*a*), by probing the fast evolving electric fields following high-intensity laser irradiation of a solid target.

3. PROTON IMAGING

Due to the advantageous properties described above, laser-produced protons are a ideal tool for probing investigations. These may include their use in conventional proton radiography (Koehler, 1968), that is, the detection via collisional stopping of aerial density variations. However in the following, we will describe a different probing application, which we have called *proton imaging* (Borghesi, 2001*a*, 2001*d*), in which the proton probe is used to probe objects much thinner than the collisional stopping distance of the protons. In this regime, the dominant effect modifying the intensity profile of the proton beam will be deflections by the e.m. fields present in the object plane. In particular, we have investigated solid targets and plasmas irradiated by ultraintense laser pulses, using probing geometries in which, due to the symmetry of the field configuration, the effect of electric fields was dominant over the effect of magnetic fields.

As the proton beam originates (or appears to) from a small source, when a thin object is placed between the source and a detector, there will be a one-to-one correspondence between the points of the object plane and of the detector plane (we assume purely geometrical propagation for the protons). Distortions to this one-to-one correspondence can be ascribed to deflections undergone by the protons when crossing the object plane, and ultimately correlated to the electric fields present in the object plane.

The broad spectral content of the beam is an advantage when probing evolving field distributions, as, due to the different propagation velocity of the various energy components, the protons will be spread temporally when they reach the object plane. As the detector performs spectral selection, each layer will convey information pertaining to different stages of the target evolution. Therefore the technique is intrinsically multiframe (Borghesi, 2001*a*).

The high temporal resolution of the diagnostic makes it ideal to study highly transient fields, such as, for example, the ones arising from the electron dynamics following intense, short pulse interactions. Such measurements were carried out by exploiting the possibility of splitting the VULCAN CPA pulse in two beams (CPA_1 and CPA_2), focusable with separate optics along separate lines. Due to setup constraints, the energy content of each pulse had to be limited to 20 J, giving intensities of about 10^{19} W/cm^2. The temporal separation of the two pulses could be varied shot to shot. The CPA_2 pulse was used to produce a proton beam from an Al foil, and the proton beam was used to probe, transversely, the interaction of the CPA_1 pulse with solid targets or preformed plasmas.

As an example, in Figure 4 proton images taken after the ultraintense irradiation of a 150-μm glass microballoon are shown. The three images are obtained on three consecutive layers of RC film in a single shot, and provide an example of

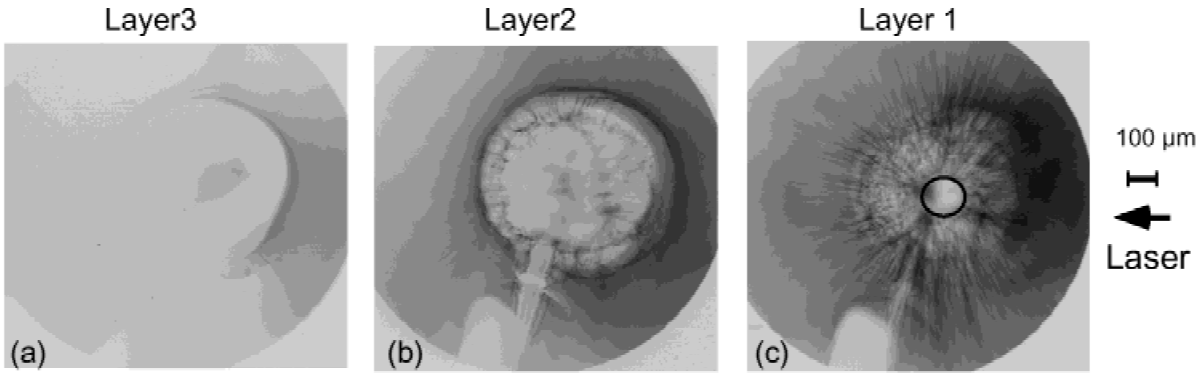

Fig. 4. Proton images taken following CPA irradiation of a 150-μm glass microballoon. The original size and position of the target are indicated by the black circle in (c). Each picture refers to subsequent RCF layers (i.e., different proton energy Ep and different probing delay Δt from the interaction): (a) $Ep \sim 8$ MeV, $\Delta t \sim 0$; (b) $Ep \sim 6$–7 MeV, $\Delta t \sim 10$ ps; (c) $Ep \sim 3$–5 MeV, $\Delta t \sim 20$–35 ps.

https://doi.org/10.1017/S0263034602202177 Published online by Cambridge University Press

the multiframe property of the diagnostic. In coincidence with the interaction, a shadow, much larger than the target, appears in the image. This is consistent with proton deflection due to an outwardly directed electric field, caused by positive charging of the microballoon as fast electrons are expelled from the target during the interaction. By matching the deflection to the calculated deflection for protons propagating in a Coulomb field, we have obtained the first measurement of positive whole target charge-up due to the expulsion of fast electrons during the interaction (Borghesi, 2001*b*). The charge at $t = 0$ was estimated to be $Q \sim 2 \times 10^{-8}$ C. The corresponding electric field at the target surface is $E \sim 10^{10}$ V/m. A rapid discharge was observed, likely to be due to the return into the target of some of the hot electrons previously expelled. The data also show deflections caused by filamentary field structures, which have been associated with the growth of an electromagnetic instability of the hot electron current flowing back into the target. More details about these results and other important observations obtained with this diagnostic setup (which cannot be discussed here due to space constraints) are provided in other publications (Borghesi, 2001*a*, 2001*b*, 2001*c*, 2001*d*; Schiavi, 2001).

4. CONCLUSION

Proton beams produced during ultraintense interaction with solid foils have been characterized in view of their application as a particle beam probe for laser–plasma interaction experiments. The properties of the proton beams can be successfully exploited as a diagnostic, for example, for imaging field distributions inside laser-produced plasmas or in the vicinity of laser-irradiated targets. The first applications of this novel technique have been carried out, leading for the first time to direct detection of electric fields during laser–plasma interactions.

ACKNOWLEDGMENTS

The work was supported by an Engineering and Physical Sciences Research Council grant, a Laboratory Directed Research and Development grant, and an Industrial Research and Technology Unit-Europe Network grant. We acknowledge the invaluable contribution to the work provided by the Central Laser Facility staff at the RAL, and by the JanUSP staff at LLNL. We also acknowledge the theoretical contribution to the project of Prof. M.G. Haines (Imperial College, London, UK) and Dr. H. Ruhl (General Atomics, San Diego, CA).

REFERENCES

Borghesi M., Campbell, D.H., Haines, M.G., Schiavi, A., Willi, O., Mackinnon, A.J., Galimberti, M., Gizzi, L.A., Clarke, R.J., Hawkes, S. & Ruhl, H. (2001*a*). In *Central Laser Facility Rutherford Appleton Laboratory Annual Report 2000–2001,* RAL-TR-2001-030, pp. 4–6 (http://www.clf.rl.ac.uk/Report/2000-2001/pdf/6.pdf).

Borghesi, M., Campbell, D.H., Schiavi, A., Willi, O., Mackinnon, A.J., Galimberti, M., Gizzi, L.A., Clarke, R.J., Hawkes, S. & Ruhl, H. (2001*b*). In *Central Laser Facility Rutherford Appleton Laboratory Annual Report 2000–2001,* RAL-TR-2001-030, pp. 7–9 (http://www.clf.rl.ac.uk/Report/2000-2001/pdf/7.pdf).

Borghesi, M., Campbell, D.H., Schiavi, A., Willi, O., Ruhl, H., Naumova, N., Pegoraro, F., Bulanov, S., Mackinnon, A.J., Galimberti, M., Gizzi, L.A., Clarke, R.J. & Hawkes, S. (2001*c*). In *Central Laser Facility Rutherford Appleton Laboratory Annual Report 2000–2001,* RAL-TR-2001-030, pp. 10–12 (http://www.clf.rl.ac.uk/Report/2000–2001/pdf/8.pdf).

Borghesi, M., Schiavi, A., Campbell, D.H., Haines, M.G., Willi, O., Mackinnon, A.J., Gizzi, L.A., Galimberti, M., Clarke, R.J. & Ruhl, H. (2001*d*). *Plasma Phys. Control Fusion* **43**, A267.

Clark, E.L, Krushelnick, K., Davies, J.R., Zepf, M., Tatarakis, M., Beg, F.N., Machacek, A., Norreys, P.A., Santala, M.I.K., Watts, I. & Dangor, A.E. (2000). *Phys. Rev. Lett.* **84**, 670–673.

Fews, A.P. & Henshaw, D.L. (1982). *Nucl. Instrum. Methods Phys. Res.* **197**, 512–529.

Fews, A.P., Norreys, P., Beg, F.N., Bell, A.R., Dangor, A.E., Danson, C.N., Lee, P. & Rose, S.J. (1994). *Phys. Rev. Lett.* **73**, 1801–1804.

Gitomer, S.J., Jones, R.D., Begay, F., Ehler, A.W., Kephart, J.F. & Kristal, R. (1986). *Phys. Fluids* **29**, 2679–2687.

Hatchett, S.P., Brown, C.G., Cowan, T.E., Henry, E.A., Johnson, J.S., Key, M.H., Koch, J.A., Langdon, A.B., Lasinski, B.F., Lee, R.W., Mackinnon, A.J., Pennington, D.M., Perry, M.D., Phillips, T.W., Roth, M., Sangster, T.C., Singh, M.S. & Yasuike, R. (2000). *Phys. Plasmas* **7**, 2076–2082.

Koehler, A.M. (1968). *Science* **160**, 303–305.

Mackinnon, A.J., Borghesi, M., Hatchett, S., Key, M.H., Patel, P., Campbell, D.H., Schiavi, A., Snavely, R. & Willi, O. (2001*a*). *Phys. Rev. Lett.* **86**, 1769–1773.

Mackinnon, A.J., Patel, P.K., Hatchett, S., Key, M.H., Lasinski, B., Langdon, B., Sentoku, Y., Andersen, C., Snavely, S. & Freeman, R.R. (2001*b*). *Bull. Am. Phys. Soc.* **46**, 253.

Maksimchuk, A., Gu, S., Flippo, K., Umstadter, D. & Bychenkov, V.Yu. (2000). *Phys. Rev. Lett.* **84**, 4108–4111.

McLaughlin, W.L., Yundong, C., Soares, C.G., Miller, A., VanDyk, G. & Lewis, D.F. (1991). *Nucl. Instr. Methods Phys. Res. A* **302**, 165–176.

Nemoto, K., Maksimchuk, A., Banerjee, S., Flippo, K., Mourou, G., Umstadter, D. & Bychenkov, V.Yu. (2001). *Appl. Phys. Lett.* **78**, 595–597.

Pukhov, A. (2001). *Phys. Rev. Lett.* **86**, 3562–3565.

Ruhl, H., Bulanov, S.V., Cowan, T.E., Liseikina, T.V., Nickles, P., Pegoraro, F., Roth, M. & Sandner, W. (2001). *Plasma Phys. Rep.* **27**, 363–371.

Schiavi, A., Campbell, D.H., Willi, O., Borghesi, M. & Ruhl, H. (2001). In *Proceedings of the 28th EPS Conference on Controlled Fusion and Plasma Physics,* P5.077, Funchal, Portugal (http://www.cfn.ist.utl.pt/EPS2001/fin/).

Snavely, R.A., Key, M.H., Hatchett, S.P., Cowan, T.E., Roth, M., Phillips, T.W., Stoyer, M.A., Henry, E.A., Sangster, T.C., Singh, M.S., Wilks, S.C., Mackinnon, A., Offenberger, A., Pennington, D.M., Yasuike, K., Langdon, A.B., Lasinski, B.F., Johnson, J., Perry, M.D. & Campbell, E.M. (2000). *Phys. Rev. Lett.* **85**, 2945–2948.

Zepf, M., Clark, E.L., Krushelnick, K., Beg, F.N., Escoda, C., Dangor, A.E., Santala, M.I.K., Tatarakis, M., Watts, I.F., Norreys, P., Clarke, R.J., Davies, J.R., Sinclair, M.A., Edwards, R.D., Goldsack, T.J., Spencer, I. & Ledingham, K.W.D. (2001). *Phys. Plasmas* **8**, 2323–2330.

https://doi.org/10.1017/S0263034602202177 Published online by Cambridge University Press